Solid-State Electronics 52 (2008) 1861–1866

Contents lists available at ScienceDirect

Solid-State Electronics

journal homepage: www.elsevier.com/locate/sse

Electron subband structure and controlled valley splitting in silicon thin-body SOI FETs: Two-band k · p theory and beyond

Viktor Sverdlov *, Siegfried Selberherr

Institute for Microelectronics, Technische Universität Wien, Gußhausstraße 27-29/E360, 1040 Vienna, Austria

ARTICLE INFO

Article history:
Received 17 March 2008
Received in revised form 28 April 2008
Accepted 13 June 2008
Available online 26 October 2008

The review of this paper was arranged by Dimitri Lederer and Jean-Pierre Colinge

Keywords:
Two-band **k** · **p** model
Tight-binding model
Stress engineering
Controllable valley splitting

ABSTRACT

We use a two-band **k** · **p** Hamiltonian to describe the subband structure in strained silicon thin films. The model describes the dependence of the transversal effective mass on strain and film thickness. However, it is found that the two-band **k** · **p** model is unable to describe recently observed large valley splitting. Therefore a generalization of the model is necessary. To go beyond the **k** · **p** theory, an auxiliary tight-binding model defined on a lattice of sites containing two localized orbitals is introduced in such a way that it reproduces the bulk dispersion obtained from the two-band **k** · **p** model. Corresponding dispersion relations including strain are obtained. We discuss an alternative mechanism to create and control the valley splitting by applying shear strain. The valley splitting increases with increased shear strain and decreasing film thickness and can be larger than the spin splitting. This makes silicon-based quantum devices promising for future applications in quantum computing.

1. Introduction

Downscaling of MOSFETs as institutionalized by Moore's law is successfully continuing because of innovative changes in the technological processes and the introduction of new materials. The 45 nm MOSFET process technology recently developed by Intel [1] involves new hafnium-based high-*k* dielectric/metal gates and represents a major change in the technological process since the invention of MOSFETs. Although alternative channel materials with a mobility higher than in Si were already investigated [2,3], it is believed that strained Si will be the main channel material for MOSFETs beyond the 45 nm technology node [3].

A multi-gate MOSFET FinFET architecture is expected to be introduced for the 22 nm technology node. Combined with a high-*k* dielectric/metal gate technology and strain engineering, a multi-gate MOSFET appears to be the ultimate device for high-speed operation with excellent channel control, reduced leakage currents, and low power budget. Confining carriers within thin Si films reduces the channel dimension in transversal direction, which further improves gate channel control. The quantization energy in ultra-thin Si films may reach a (few) hundred(s) meV. The parabolic conduction band approximation usually employed for subband structure calculations of confined electrons in Si inversion layers may turn out to be insufficient in ultra-thin Si films. A recent study of subband energies in (001) and (110) oriented thin Si films reveals that even the non-parabolic isotropic dispersion is not sufficient to describe experimental data, and a direction-dependent anisotropic non-parabolicity must be introduced [4].

The two-band **k** · **p** model [5–8] provides a general approach to compute the subband structure, in particular the dependence of the electron effective masses on shear strain. In case of a square potential well with infinite walls, which is a good approximation for the confining potential in ultra-thin Si films, the subband structure can be obtained analytically [9]. This allows an analysis of subband energies and dispersion on film thickness for arbitrary stress conditions. On the other hand, the traditional **k** · **p** method has shortcomings when describing the subband structure in strained Si films. The most obvious limitation is the inability to address the splitting between the subbands belonging to equivalent valleys. Indeed, due to the valley degeneracy, the unprimed subbands in (001) Si films remain two-times degenerate within the **k** · **p** approach. However, an experimental observation of valley splitting larger than the spin splitting was reported recently [10]. It is therefore necessary to go beyond the **k** · **p** theory by restoring some of the important properties of the periodic Bloch amplitude, which is ignored in a **k** · **p** treatment, because the Bloch amplitudes enter into the **k** · **p** theory only in integral form via parameters of the model.

In the following we briefly review the main ideas behind the two-band **k** · **p** model for a valley in the conduction band of Si. We will shortly analyze the unprimed subband structure in (001) ultra-thin Si films, stressing the advantages of the subband description based on the two-band **k** · **p** model and discussing its limitations. Then the Bloch amplitude will be introduced into the envelope wave

* Corresponding author. Tel.: +43 1 58801 36033; fax: +43 1 58801 36099.
E-mail address: sverdlov@iue.tuwien.ac.at (V. Sverdlov).

0038-1101/$ - see front matter © 2008 Elsevier Ltd. All rights reserved.
doi:10.1016/j.sse.2008.06.054

function of an electron in the conduction band. The Bloch amplitude is deduced from a tight-binding model with two orbitals per site, which mimics dispersion relations of the underlying two-band $\mathbf{k}\cdot\mathbf{p}$ theory. The total wave function including the Bloch amplitude describes the energy splitting between the two unprimed subband ladders generic to the two equivalent conduction band valleys in an ultra-thin Si film. Lifting degeneracy between the two valleys reduces scattering and improves the coherence time in Si-based spin qubits, which makes silicon-based quantum devices promising for future applications in quantum computing [10]. We demonstrate that the valley splitting in (0 0 1) Si films can be controlled and significantly enhanced by applying stress in [1 1 0] direction.

2. Uniaxial stress and conduction band structure

From symmetry consideration it follows that the two-band $\mathbf{k}\cdot\mathbf{p}$ Hamiltonian of a [0 0 1] valley in the vicinity of the X-point of the Brillouin zone in Si must be in the form [6]:

$$H=\left(\frac{\hbar^2k_z^2}{2m_\mathrm{l}}+\frac{\hbar^2(k_x^2+k_y^2)}{2m_\mathrm{t}}\right)I+\left(D\varepsilon_{xy}-\frac{\hbar^2k_xk_y}{M}\right)\sigma_z+\frac{\hbar^2k_zk_0}{m_\mathrm{l}}\sigma_y, \quad (1)$$

where $\sigma_{y,z}$ are the Pauli matrixes, I is the 2×2 unity matrix, m_t and m_l are the transversal and the longitudinal effective masses, $k_0=0.15\times2\pi/a$ is the position of the valley minimum relative to the X-point in unstrained Si, ε_{xy} denotes the shear strain component in physics notations, $M^{-1}\approx m_\mathrm{t}^{-1}-m_0^{-1}$, and $D=14$ eV is the shear strain deformation potential [5–8]. The two-band Hamiltonian results in the following dispersions [6]:

$$E=\frac{\hbar^2k_z^2}{2m_\mathrm{l}}+\frac{\hbar^2(k_x^2+k_y^2)}{2m_\mathrm{t}}\pm\sqrt{\left(\frac{\hbar^2k_zk_0}{m_\mathrm{l}}\right)^2+\delta^2}, \quad (2)$$

where the negative sign corresponds to the lowest conduction band,

$$\delta^2=(D\varepsilon_{xy}-\hbar^2k_xk_y/M)^2. \quad (3)$$

We stress that the k_z moment as well as energies in (2) are counted from the X-point of the Brillouin zone. The usual parabolic approximation is obtained from (2), when coupling between the two conduction bands described by the parameter δ is neglected. Coupling between the bands is small, when the wave vectors $|k_x|$, $|k_y|\ll k_0\,(M/m_\mathrm{l})^{1/2}$ and shear stress $\varepsilon_{xy}=0$. Due to band coupling the dispersion (2) becomes non-parabolic in stressed Si, if the shear strain component is non-zero, and/or at higher energies. In order to verify the accuracy of (2) we have carried out numerical band structure calculations with the empirical pseudo-potential method (EPM) with parameters from [7,11]. Excellent agreement between the two-band $\mathbf{k}\cdot\mathbf{p}$ model (1) and the EPM results was confirmed up to energy 0.5 eV.

Tensile stress in [1 1 0] and compressive stress in orthogonal [−1 1 0] direction of 150 MPa are applied resulting in only a non-zero ε_{xy} shear strain component. Shear strain ε_{xy} substantially modifies the energy dispersion of the [0 0 1] valleys even at small energies making the dispersion relation anisotropic [5–8]. Shear strain also modifies the k_z dispersion as shown in Fig. 1 for several values of shear strain. The valley minimum moves both in energy and position, approaching the X-point of the Brillouin zone for larger strain $\varepsilon_{xy}\leqslant\hbar^2k_0^2/(m_\mathrm{l}D)$. At the same time k_z dispersion becomes highly non-parabolic.

The relation (2) is valid in a larger range of energies compared to parabolic dispersion with isotropic non-parabolic correction and can be used to determine the subband structure in thin Si films. The subband energies can be found analytically for an infinite square well potential which is a good approximation for an ultra-thin Si film. The dispersion of the unprimed subbands in a [0 0 1] thin Si film of thickness t is [9]:

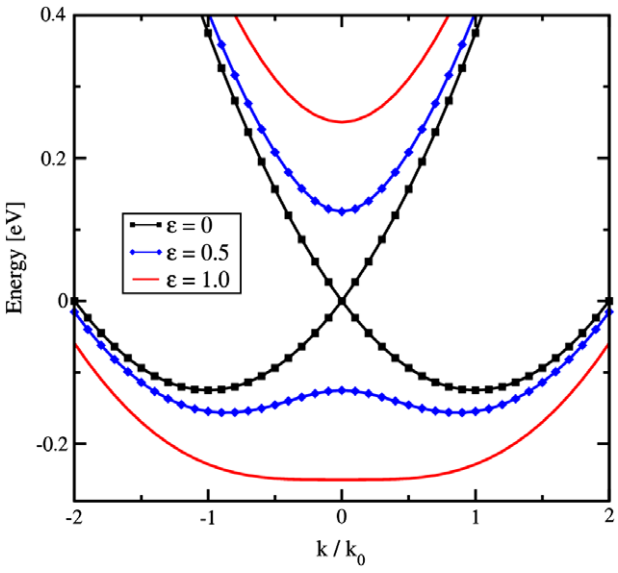

Fig. 1. Dispersion as it follows from (2). With strain increased the gap opens between the two bands at the X-point, and dispersion becomes highly non-parabolic.

$$E_n(k_x,k_y)=E_n^0(k_x,k_y)-\delta^2m_\mathrm{l}/[2\hbar^2k_0^2(1-q_n^2)], \quad (4)$$

where $q_n=(\pi n)/(tk_0)$and E_n^0 is the subband dispersion for parabolic bands:

$$E_n^0(k_x,k_y)=\frac{\hbar^2\pi^2n^2}{2m_\mathrm{l}t^2}+\frac{\hbar^2(k_x^2+k_y^2)}{2m_\mathrm{t}}-\frac{\hbar^2k_0^2}{2m_\mathrm{l}}.$$

(4) is valid when

$$(1-q_n^2)^2>\delta^2m_\mathrm{l}^2/\hbar^4k_0^4. \quad (5)$$

Dispersion (4) describes the subband quantization energy correction due to strain with respect to the valley minimum:

$$\Delta E_n(\varepsilon_{xy})=-\frac{\pi^2n^2}{2m_\mathrm{l}t^2}\frac{(D\varepsilon_{xy}m_\mathrm{l})^2}{\hbar^2k_0^4(1-q_n^2)}. \quad (6)$$

(6) is obtained after taking into account the strained induced valley minimum energy shift $\Delta E(\varepsilon_{xy})=-(D\varepsilon_{xy})^2m_\mathrm{l}/(2\hbar^2k_0^2)$ and the dependence of the longitudinal mass m_l on strain [7,8]:

$$m_\mathrm{l}(\varepsilon_{xy})=m_\mathrm{l}\left(1-(D\varepsilon_{xy}m_\mathrm{l})^2/\hbar^4k_0^4\right)^{-1}$$

(4) also describes corrections to the transversal mass m_t due to strain ε_{xy}, thickness t, and subband number n:

$$m_n^{\mp}=m_\mathrm{t}\left(1\pm\frac{D\varepsilon_{xy}m_\mathrm{l}}{\hbar^2k_0^2}\frac{m_\mathrm{t}}{M}\frac{1}{1-q_n^2}\right)^{-1}. \quad (7)$$

Here m_t^- is the effective mass along the direction [1 1 0] of tensile strain. In thin films the effective mass depends not only on strain but also on film thickness. (7) is compared to the corresponding dependence in bulk silicon in Fig. 2. The thickness dependence of the last term in (7) leads to a more pronounced anisotropy in the transversal mass than in bulk semiconductor.

A comparison of the dispersion relation (4) to the parabolic approximation with transversal masses (7) is shown in Fig. 3 (unstrained film) and Fig. 4 (strain $\varepsilon_{xy}=1\%$). Deviations from the parabolic approximation become large for electron energies above 20 meV. Therefore, to compute the carrier concentration and mobility in thin Si films the dispersion relation (4) should be used instead of a parabolic approximation at higher carrier concentrations.

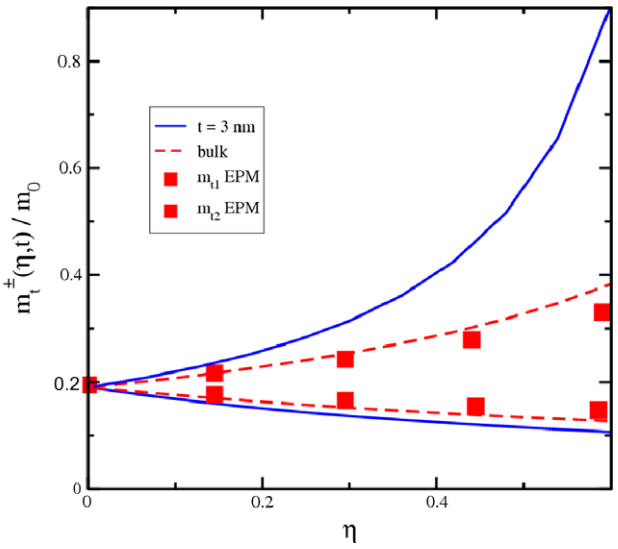

Fig. 2. Strain-modified subband effective mass (solid lines). Strain dependence of the transversal mass in bulk silicon is shown by dashed lines and symbols (results of pseudo-potential calculations).

(4) is valid only when the condition (5) is satisfied. The quantization energies obtained by setting k_x, $k_y = 0$ are shown in Fig. 5 and Fig. 6 by circles. In unstrained Si the k_z dispersion is parabolic with the minima $p_z = \pm k_0$, and the subband energies are obtained from the equation:

$$E\left(p_z - \frac{\pi n}{t}\right) = E\left(p_z + \frac{\pi n}{t}\right), \tag{8}$$

where $E(k_z)$ is determined by (2). For non-zero strain the gap at the X-point between the two conduction bands opens, and the k_z dispersion becomes non-parabolic. This results in the dependence of p_z on strain, thickness, and subband number:

$$p_z = \pm k_0 \sqrt{1 - (\delta m_l / \hbar^2 k_0^2)^2 / (1 - q_n^2)}. \tag{9}$$

The two signs in (9) correspond to two sets of subband ladders. We notice that, according to (2), (8), within the two-band $\mathbf{k}\cdot\mathbf{p}$ theory the subband energies are the same, so the two subband ladders are *degenerate*. Therefore, the two-band $\mathbf{k}\cdot\mathbf{p}$ theory is unable to describe the splitting between the two subband ladders from different valleys. This splitting was described theoretically [12] and confirmed by several numerical calculations [13,14]. It was recently demonstrated experimentally that the splitting is quite large [10]. One important limitation of the two-band $\mathbf{k}\cdot\mathbf{p}$ theory is that it cannot describe this splitting.

Another shortcoming of the $\mathbf{k}\cdot\mathbf{p}$ theory can be illustrated as follows. If the condition (5) is not fulfilled, (8) is satisfied only with $p_z = 0$. It results in a subband dispersion obtained from (2) with $k_z = \pi n/t$. These solutions shown by crosses in Fig. 6 are clearly different from those described by (9) with non-zero p_z. In reality, however, a smooth transition between them is anticipated when the parameters, in particular strain which regulates the gap, are gradually changing, and the two types of solutions will be related. However, within the $\mathbf{k}\cdot\mathbf{p}$ theory even the number of subbands is not conserved. Indeed, with the gap increased, a pair of degenerate subbands eventually reaches the maximum of the dispersion curve at the X-point, where it enters into the gap and becomes the only subband with $p_z = 0$, marked by crosses in Fig. 6. One subband becomes missing, since there is only a single solution with $p_z = 0$ within the gap. In order to accurately resolve the crossover between the two types of solutions and describe the valley splitting correctly one has to go beyond the two-band $\mathbf{k}\cdot\mathbf{p}$ theory.

3. Beyond the k · p model

We introduce an auxiliary tight-binding model defined on a lattice of sites each containing two localized orbitals $\alpha(z)$ and $\beta(z)$.

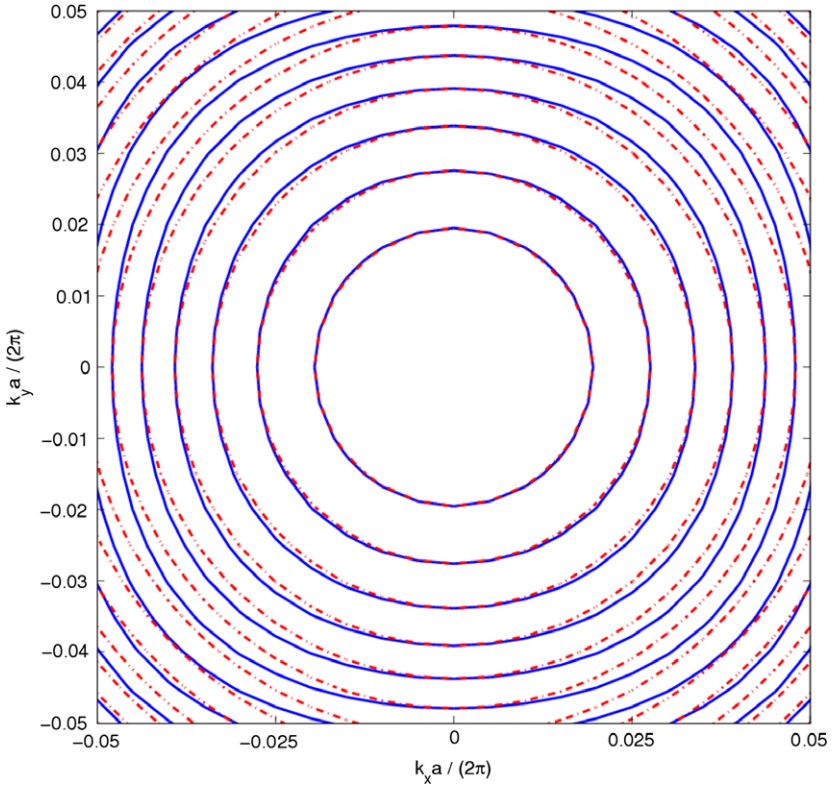

Fig. 3. Subband dispersion (4) (solid) as compared to the parabolic approximation (dotted), for film thickness $t = 5.4$ nm. Spacing between lines is 10 meV.

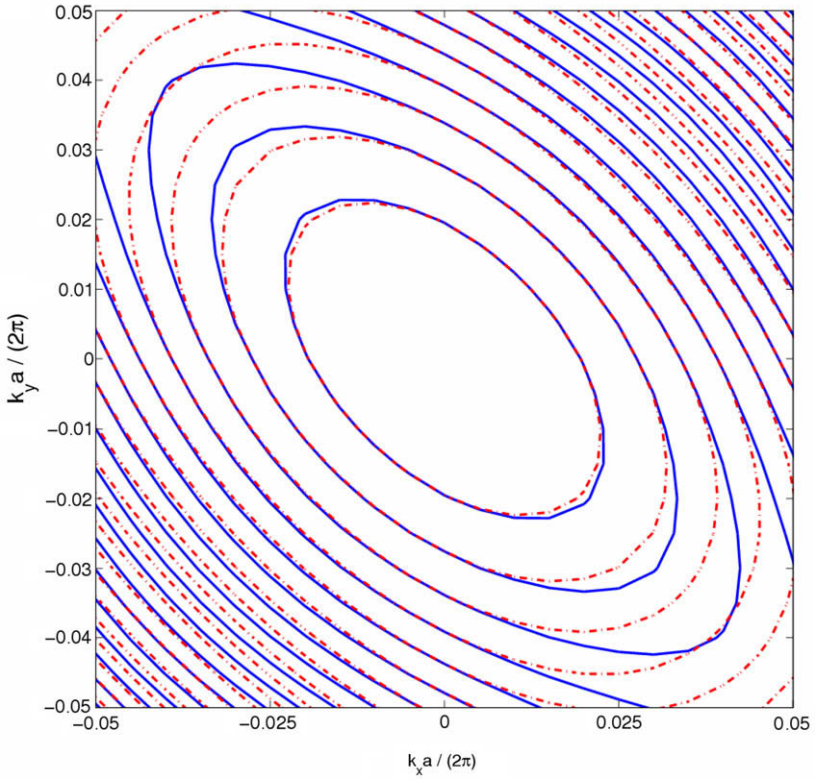

Fig. 4. Subband dispersion (4) (solid) as compared to the parabolic approximation (dotted), for a strained film of thickness t = 5.4 nm. Tensile strain of ε_{xy} = 1% is applied along [1 1 0] direction. Spacing between lines is 10 meV.

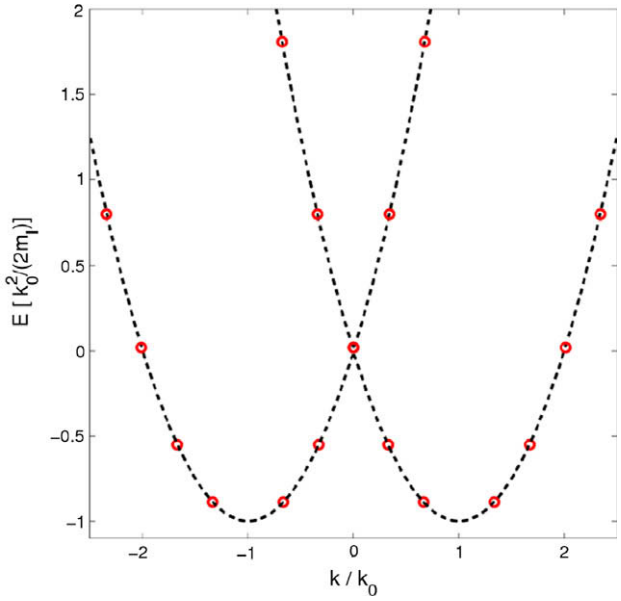

Fig. 5. Subband energies in unstrained Si film from the two-band $\mathbf{k}\cdot\mathbf{p}$ theory.

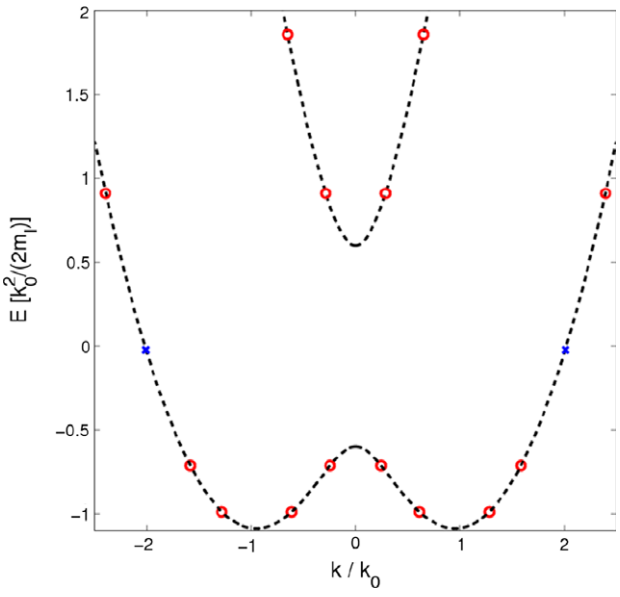

Fig. 6. Same as in Fig. 5 in a stressed Si film. The gap at the X-point leads to non-parabolic dispersion.

The Bloch functions corresponding to the bands considered within the two-band $\mathbf{k}\cdot\mathbf{p}$ theory are expressed via the two orbitals as

$$u(z)=\sum_{n=-\infty}^{\infty}\alpha(z-na/2);v(z)=\sum_{n=-\infty}^{\infty}\mathrm{i}\beta(z-na/2). \tag{10}$$

For an arbitrary wave k_z vector the Bloch function is written as [15]

$$\psi(z,k_z)=\mathrm{e}^{\mathrm{i}k_z z}(a(k_z)u(z)+b(k_z)v(z)), \tag{11}$$

where the coefficients $a(k_z)$ and $b(k_z)$ are determined from the two-band $\mathbf{k}\cdot\mathbf{p}$ Hamiltonian (1), which was rotated for convenience:

$$\begin{pmatrix} \frac{\hbar^2k_z^2}{2m_l}+\frac{\hbar^2(k_x^2+k_y^2)}{2m_t}-\delta-E & \frac{k_zk_0}{m_l} \\ \frac{k_zk_0}{m_l} & \frac{\hbar^2k_z^2}{2m_l}+\frac{\hbar^2(k_x^2+k_y^2)}{2m_t}+\delta-E \end{pmatrix}\begin{pmatrix} a(k_z) \\ b(k_z)\end{pmatrix}=0. \tag{12}$$

Here the eigenenergies E are determined by (2). We note that for $\delta = 0$ the coefficients $a(k_z)$ and $b(k_z)$ are independent on k_z and equal in absolute value. We will use this fact later.

Using (10) we can now rewrite the wave function (11) in the form

$$\psi(z,k_z)=\sum_{n=-\infty}^{\infty} e^{ik_z na/2}(a(k_z)\alpha\prime(z-na/2)+ib(k_z)\beta\prime(z-na/2)). \tag{13}$$

The primed orbital functions in (13) are related to the ones in (11) by

$$\begin{aligned}\alpha\prime(z-na/2) &= e^{ik_z(z-na/2)}a(z-na/2), \beta\prime(z-na/2)\\ &= e^{ik_z(z-na/2)}\beta(z-na/2).\end{aligned}$$

However, we neglect this difference under the assumption that the orbitals are strongly localized and the localization radius r satisfies the condition $r/a << 1$.

For the dispersion relation (2) for a particular energy E there exist two pairs of real roots $k_z = \pm k_1, \pm k_2$ for subbands with $p_z > 0$ and a pair of real $k_z = \pm k_1$ and a pair of imaginary roots $k_z = \pm i|k_2|$ for the subbands with $p_z = 0$. Then the wave functions for a finite array of $2N$ sites are

$$\begin{aligned}\psi_{\pm}(z,E)=\sum_{i=1,2}\sum_{n=-N}^{N} C_i \exp(ik_i na/2)(a(k_i)\alpha(z-na/2)\\ +ib(k_i)\beta(z-na/2))\pm \text{C.C.},\end{aligned} \tag{14}$$

where *C.C.* stands for complex conjugate. Each pair of the solution enters with its own coefficient. Within each pair $k_z = \pm k_j$ symmetric and asymmetric combinations are allowed. This is taken into account by the plus/minus sign in (14). In writing (14) we have assumed that both roots $k_1 > k_2$ are real. In case when the root k_2 is imaginary, the coefficient $b(k_2)$ is also imaginary. This corresponds to the solutions of the second type shown by crosses in Fig. 6.

Taking into account strong on-site localization of orbitals and their mutual orthogonormality, the condition that the wave function is zero at the film interfaces $z = \pm t/2$ results in two sets of equations (k_2 is real) corresponding to the minus sign in (14) [13]:

$$C_1 a(k_1)\sin(k_1 t/2)+C_2 a(k_2)\sin(k_2 t/2)=0, \tag{15a}$$

$$C_1 b(k_1)\cos(k_1 t/2)+C_2 b(k_2)\cos(k_2 t/2)=0, \tag{15b}$$

and to the plus sign in (14):

$$C_1 a(k_1)\cos(k_1 t/2)+C_2 a(k_2)\cos(k_2 t/2)=0, \tag{16a}$$

$$C_1 b(k_1)\sin(k_1 t/2)+C_2 b(k_2)\sin(k_2 t/2)=0. \tag{16b}$$

(15) results in the following dispersion relation:

$$\tan\left(k_1\frac{t}{2}\right)=\frac{a(k_2)}{b(k_2)}\frac{b(k_1)}{a(k_1)}\tan\left(k_2\frac{t}{2}\right), \tag{17a}$$

while (16) gives:

$$\cot\left(k_1\frac{t}{2}\right)=\frac{a(k_2)}{b(k_2)}\frac{b(k_1)}{a(k_1)}\cot\left(k_2\frac{t}{2}\right). \tag{17b}$$

Since k_1 and k_2 are the solution of the dispersion relation (2) for the same energy E, they are related by:

$$k_2^2=k_1^2+4-4\sqrt{k_1^2+\frac{\delta^2 m_l^2}{\hbar^4 k_0^4}}. \tag{18}$$

Substitution of (18) into (17) results in the equations for k_1 alone. When the solutions for k_1 are found, the subband energies are computed using the dispersion relation (2).

Eqs. (17) and (18) are highly nonlinear and can only be solved numerically. However, the asymptotic behavior of their solutions can be analyzed analytically. We investigate the solutions close to the transition between the two types of subbands discussed above. This transition occurs when k_2 is very close to the X-point and is therefore extremely small. As an example we consider the situation when both k_1 and k_2 correspond to the branch with a minus sign in (2), when the energy E is approaching the gap from below. For small $k_2 t << 1$

$$\frac{a(k_2)}{b(k_2)}\approx\frac{k_2 k_0}{2\delta m_l},\quad \tan(k_2 t/2)\approx k_2 t/2,$$

and (17) is written as

$$\tan\left(k_1\frac{t}{2}\right)\approx\frac{b(k_1)}{a(k_1)}\frac{k_2^2 k_0 t}{4\delta m_l}\to 0; \tag{18a}$$

$$\cot\left(k_1\frac{t}{2}\right)\approx\frac{b(k_1)}{a(k_1)}\frac{k_0}{t\delta m_l}. \tag{18b}$$

When k_2 goes to zero, (18a) gives $k_1 = 2\pi n/t$. The solution of (18b) depends on the system parameters. In weakly stressed thin films, where the parameter $\hbar^2 k_0/(t\delta m_l) >> 1$, (18b) gives $k_1 = 2\pi n/t$, and the subbands (18b) are nearly degenerate with those given by (18a). In the opposite limiting case $\hbar^2 k_0/(t\delta m_l) << 1$ (18b) provides the usual complimentary solution $k_1 = 2\pi(n+1/2)/t$ corresponding to odd subbands.

When the subband energy lies in the gap and k_2 is imaginary, equations for k_1 take the form:

$$\tan\left(k_1\frac{t}{2}\right)=\frac{a(k_2)}{|b(k_2)|}\frac{b(k_1)}{a(k_1)}\tanh(|k_2|\frac{t}{2}), \tag{19a}$$

$$\cot(k_1\frac{t}{2})=\frac{a(k_2)}{|b(k_2)|}\frac{b(k_1)}{a(k_1)}\coth(|k_2|\frac{t}{2}), \tag{19b}$$

In contrast to Eq. (18), the (19) contain the hyperbolic functions in the right-hand side as well as the absolute values of the complex valued functions k_2 and $b(k_2)$. However, in the limit $k_2 t << 1$ the (19) have exactly the same asymptotic behavior of the solutions as (18). Therefore, Eqs. (18)and (19) are able to continuously describe the transition between the two types of subbands when the solution enters into the gap. Since the number of subbands is conserved, the theory based on the wave function (14) is free of this limitation of the $\mathbf{k}\cdot\mathbf{p}$ model discussed above.

It is interesting to recover results corresponding to a single parabolic band from the two-band expressions (19). The single parabolic band is obtained from (2) when the limit $\delta \gg \hbar^2 k_0^2/m_l$ is taken. In this limit we get from (18) $\hbar k_2 = 2\sqrt{-m_l\delta}$, and it then follows from (19):

$$\tan\left(k_1\frac{t}{2}\right)\approx\frac{b(k_1)}{a(k_1)}\frac{\hbar k_0}{\sqrt{\delta m_l}}\to 0 \tag{20a}$$

$$\cot\left(k_1\frac{t}{2}\right)\approx\frac{b(k_1)}{a(k_1)}\frac{\hbar k_0}{\sqrt{\delta m_l}}\to 0. \tag{20b}$$

Therefore, for large δ we obtain from (20) the well-known quantization result $k_1 = \pi n/t$ for subbands in an infinite potential square well with a single parabolic band.

4. Strain-induced valley splitting

In order to describe the valley splitting, it is convenient to introduce a new variable $y_n = (k_1 - k_2,)/(2k_0)$. The dispersion Eq. (18) are then written as

$$\sin(y_n k_0 t)=\pm\frac{\eta y_n \sin\left(\frac{1-\eta^2-y_n^2}{1-y_n^2}k_0 t\right)}{\sqrt{(1-y_n^2)(1-\eta^2-y_n^2)}}, \tag{21}$$

where dimensionless strain $\eta = m_l D\varepsilon_{xy}/(\hbar k_0)^2$ is defined. This equation represents the main result and is analyzed below.

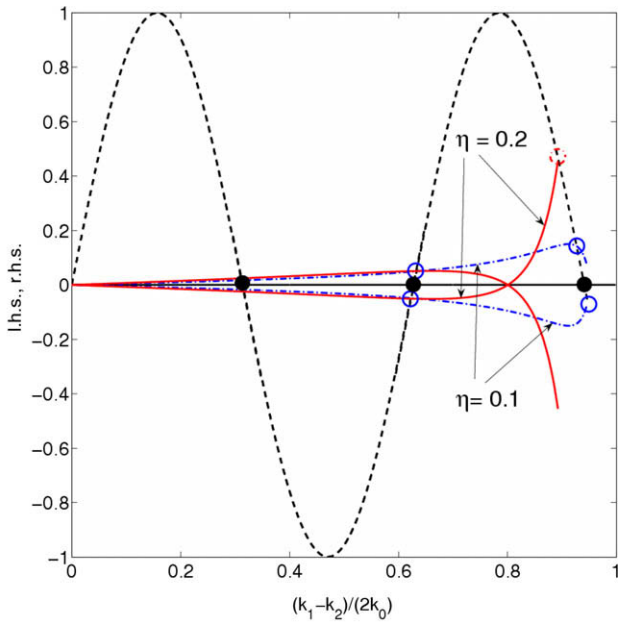

Fig. 7. The valleys are two-fold degenerate (filled circles) without strain. For non-zero shear strain the degeneracy is lifted.

It follows from (21) that in unstrained films $\eta = 0$, when the dispersion is purely parabolic, the right-hand side of (21) is zero. Therefore, for parabolic dispersion the valley splitting is exactly zero for arbitrary film thickness. Similar results could have been obtained directly from (18): as discussed, for $\eta = 0$ the coefficients $a(k_z)$ and $b(k_z)$ are equal in absolute value and cancel out from the equations, after which the standard quantization condition

$$y_n = q_n = \pi n/(k_0 t) \tag{22}$$

is recovered from both Eq. (18).

In strained films $\eta \neq 0$, the right-hand side of (21) is shown in Fig. 7, together with the left-hand side of (21). Due to the ± sign in the right-hand side a two-fold degenerate solution (22) for y_n, which corresponds to an unstrained film, splits into two non-equivalent roots for $\eta \neq 0$ and non-parabolic bands. Eq. (21) is non-linear and can be solved only numerically. However, for small η the solution can be sought in the form $y_n = q_n \pm \zeta$, where ζ is small. Substituting $y_n = q_n$ into the right-hand side of (21) and solving the equation with respect to ζ, we obtain for the valley splitting:

$$\Delta E_n = 2\left(\frac{\pi n}{k_0 t}\right)^2 \frac{D\varepsilon_{xy}}{k_0 t}\sin(k_o t). \tag{23}$$

In accordance with earlier publications [12–14], the valley splitting is inversely proportional to the third power of k_0 and the third power of film thickness t. The value of the valley splitting oscillates with film thickness, in accordance with [13,14]. In contrast to previous works, the subband splitting is proportional to the gap δ at the X-point, and not at the Γ-point. Since the parameter η, which determines non-parabolicity, depends strongly on shear strain, the application of uniaxial [1 1 0] stress to [0 0 1] ultra-thin Si film generates a valley splitting proportional to strain. Uniaxial stress is currently used to enhance performance of modern MOSFETs, where it is introduced in a controllable way. Therefore, the valley splitting (23) can be controlled by adjusting strain and thickness t.

5. Conclusion

Limitations of the two-band $\mathbf{k}\cdot\mathbf{p}$ model used for electron subband description in thin Si are discussed. One important shortcoming is the inability of the model to describe the experimentally observed valley splitting. A generalization of the two-band $\mathbf{k}\cdot\mathbf{p}$ model is suggested based on a wave function introduced with help of a tight-binding model. Dispersion relations obtained with help of this wave function are free from all limitations of the two-band $\mathbf{k}\cdot\mathbf{p}$ model and describe valley splitting in strained Si films. An alternative way to induce a large controllable valley splitting in ultra-thin Si films by applying uniaxial stress is proposed. For small stress values the splitting is shown to depend linearly on shear strain. Valley splitting rapidly increases with decreasing Si thickness and can be larger than the spin splitting.

Acknowledgement

This work was supported in part by the Austrian Science Fund FWF, project P17285-N02, and by the EUROSOI+ Thematic Network on SOI Technology, Devices and Circuits.

References

[1] Mistry K, Allen C, Beattie AB, et al. A 45 nm logic technology with high-*k*+metal gate transistors, strained silicon, 9 Cu interconnect layers, 193 nm dry patterning, and 100% Pb-free packaging. Technical Digest IEDM; 2007. p. 247–50.
[2] Hudati MK, Dewey G, Datta S, et al. Heterogeneous integration of enhancement mode $In_{0.7}Ga_{0.3}$ as quantum well transistor on silicon substrate using thin (<2 um) composite buffer architecture for high-speed and low-voltage (0.5 V) logic applications. Technical Digest IEDM; 2007. p. 625–28.
[3] Chau R. Challenges and opportunities of emerging nanotechnology for future VLSI nanoelectronics. Technical Digest ISDRS; 2007. ISBN: 978-1-4244-1892-3.
[4] Uchida K, Kinoshita A, Saitoh M. Carrier transport in (1 1 0) nMOSFETs: subband structures, non-parabolicity, mobility characteristics, and uniaxial stress engineering. Technical Digest IEDM; 2006. p. 1019–21.
[5] Hensel JC, Hasegawa H, Nakayama M. Cyclotron resonance in uniaxially stressed silicon. II. Nature of the covalent bond. Phys Rev 1965;138:A225–38.
[6] Bir GL, Pikus GE. Symmetry and strain-induced effects in semiconductors. NY: John Willey & Sons; 1974.
[7] Ungersboeck E, Dhar S, Karlowatz G, et al. The effect of general strain on the band structure and electron mobility of silicon. IEEE T Electron Dev 2007;54:2183–90.
[8] Sverdlov V, Ungersboeck E, Kosina H, Selberherr S. Effects of shear strain on the conduction band in silicon: an efficient two-band $k\cdot p$ Theory. Technical Digest ESSDERC; 2007. ISBN: 1-4244-1124-6: 386–89.
[9] Sverdlov V, Karlowatz G, Dhar S, et al. Two-band $k\cdot p$ model for the conduction band in silicon: impact of strain and confinement on band structure and mobility. Proceedings ISDRS; 2007. ISBN: 978-1-4244-1892-3.
[10] Goswami S, Slinker KA, Friesen M, et al. Controllable valley splitting in silicon quantum devices. Nat Phys 2007;3:41–5.
[11] Rieger M, Vogl P. Electronic-band parameters in strained Si_{1-x} Ge_x alloys on Si_{1-y} Ge_y substrates. Phys Rev B 1993;48:14275–87.
[12] Ando T, Fowler AB, Stern F. Electronic properties of two-dimensional systems. Rev Mod Phys 1982;54:437–672.
[13] Boykin TB, Klimeck G, Friesen M, et al. Valley splitting in low-density quantum-confined heterostructures studied using tight-binding models. Phys Rev B 2004;70:165325-1–165325-12.
[14] Esseni D, Palestri P. Linear combination of bulk bands method for investigating the low-dimensional electron gas in nanostructured devices. Phys Rev B 2005;72:165342-1–165342-14.
[15] Luttinger JM, Kohn W. Motion of electrons and holes in perturbed periodic fields. Phys Rev 1995;97:869–83.